

CHORUS

This is the accepted manuscript made available via CHORUS. The article has been published as:

Hysteretic phase transition sequence in $0.67\text{Pb}(\text{Mg}_{1/3}\text{Nb}_{2/3})\text{O}_3 - 0.33\text{PbTiO}_3$ single crystal driven by electric field and temperature

Limei Zheng, Xiaoyan Lu, Hengshan Shang, Zengzhe Xi, Ruixue Wang, Junjun Wang, Peng Zheng, and Wenwu Cao

Phys. Rev. B **91**, 184105 — Published 8 May 2015

DOI: [10.1103/PhysRevB.91.184105](https://doi.org/10.1103/PhysRevB.91.184105)

Hysteretic phase transition sequence in $0.67\text{Pb}(\text{Mg}_{1/3}\text{Nb}_{2/3})\text{O}_3$ - 0.33PbTiO_3 single crystal driven by electric field and temperature

Limei Zheng,¹ Xiaoyan Lu,² Hengshan Shang,¹ Zengzhe Xi,³ Ruixue Wang,¹
Junjun Wang,¹ Peng Zheng⁴ and Wenwu Cao^{1,5,*}

¹Condensed Matter Science and Technology Institute, Harbin Institute of Technology, Harbin 150080, China

²Key Lab of Structures Dynamic Behavior and Control of the Ministry of Education, School of Civil Engineering, Harbin Institute of Technology, Harbin 150001, China

³Shaanxi Key Laboratory of Photoelectric Functional Materials and Devices, School of Materials and Chemical Engineering, Xi'an Technological University, Xi'an 710032, China

⁴College of Electronics and Information, Hangzhou Dianzi University, Hangzhou 310018, China

⁵Department of Mathematics and Materials Research Institute, The Pennsylvania State University, University Park, Pennsylvania 16802, USA

*Corresponding author: Wenwu Cao, email: dzk@psu.edu, Phone: 1 (814) 865-4101, Fax: 1 (814) 865-2326

Abstract

Domain pattern variations with temperature were studied by polarizing light microscopy for the morphotropic phase boundary (MPB) composition $0.67\text{Pb}(\text{Mg}_{1/3}\text{Nb}_{2/3})\text{O}_3$ - 0.33PbTiO_3 (PMN-0.33PT) single crystal. At room **temperature**, the monoclinic M_A phase is the dominant phase in the unpoled crystal, which coexists with a small fraction of the tetragonal (T) phase. The **orientation of** spontaneous polarization was calculated to be around 4.8° away from the pseudo-cubic $\langle 111 \rangle_C$ in the $\{001\}_C$ plane family. Under an electric field of 6 kV/cm along $[011]_C$, a single domain orthorhombic (O) phase **was** induced, but partially switched back to M_A a few hours after the removal of the E -field. It was found that

the temperature induced phase transition sequence of the $[011]_C$ poled PMN-0.33PT single crystal is strongly hysteretic. On heating, the phase transition sequence is as follows: coexistence of O phase and monoclinic $M_A \rightarrow$ rhombohedral (R) \rightarrow monoclinic $M_C \rightarrow$ cubic (C), while on cooling, the phase transition sequence is given by: C \rightarrow T \rightarrow M_A . The complete set of dielectric, piezoelectric and elastic constants for the $[011]_C$ poled PMN-0.33PT single crystal was measured, which showed strong feature of the single domain O phase with high shear ($d_{15}=2321$ pC/N, $d_{24}=1941$ pC/N) and low longitudinal piezoelectric coefficients ($d_{33}=165$ pC/N).

Keywords: hysteretic phase transition, PMN-PT, ferroelectric, domain engineering

PACS number(s): 77.84.Cg, 77.80.B-, 77.80.Dj

I. INTRODUCTION

$(1-x)\text{Pb}(\text{Mg}_{1/3}\text{Nb}_{2/3})\text{O}_3-x\text{PbTiO}_3$ (PMN- x PT) and $(1-x)\text{Pb}(\text{Zn}_{1/3}\text{Nb}_{2/3})\text{O}_3-x\text{PbTiO}_3$ (PZN- x PT) have attracted much attention in recent years as high performance ultrasonic transducer and piezoelectric actuator materials [1-4]. Large functional properties are usually related to the morphotropic phase boundary (MPB), which separates the rhombohedral (R) and tetragonal (T) phases in the solid solution system [5-7]. The phase structure of the MPB composition materials is very complicated, and may change greatly with environmental conditions, such as electric field, stress and temperature [8-10]. Crystal structure studies on $\text{Pb}(\text{Zr}, \text{Ti})\text{O}_3$, PZN-PT and PMN-PT systems revealed the existence of an intermediate ferroelectric monoclinic (M) phase, sandwiched between the R and T phases in the phase diagram near the MPB [11-14]. Interestingly, two different types of M phases have been reported in polycrystalline ceramics and single crystal PMN-PT, i.e., M_A with the space group of Cm and M_C with the space group of Pm [6,12,15]. Some researchers even reported the coexistence of R, T and M phases in the MPB composition, which makes the domain structure more complicated, but some interesting properties may be produced due to such phase coexistence [11].

Based on synchrotron X-ray diffraction results at room temperature, Ye et al reported the existence of an M_A -type monoclinic phase in the $[001]_C$ poled PMN-0.35PT single crystal [16], while an M_C -type monoclinic phase had been found in unpoled PMN-PT ceramics [17]. The coexistence of R and M phases was confirmed by optical microscopy in PMN-0.33PT single crystals [17]. All of these structural studies were performed on $[001]_C$ oriented or $[001]_C$ poled PMN-PT single crystals. Limited studies on $[011]_C$ poled sample had been reported so far. Lu et al reported that a multidomain R phase was observed in the $[011]_C$ poled PMN-0.33PT single crystal with a poling electric field $E < 4$ kV/cm. When $E > 5$ kV/cm, a single domain orthorhombic (O) phase may be obtained [18]. Zhang et al reported that single domain O phase can be achieved in PT-based relaxor single crystals after poling along $[011]_C$ [19,20]. They have measured several full sets of material constants for the

‘single domain’ O phase. However, up to date, the phase transition sequence and rotation paths of the spontaneous polarizations (P_S) during the application of a $[011]_C$ E -field are still **unclear**. Besides, the stability of this single domain O phase after the removal of poling field has **not been studied**, i.e., the aging property of the O phase is unknown. We report here a comprehensive study on the transition sequence of poled and unpoled PMN-PT single crystals and try to understand the **phase stability of different phases in the MPB composition**. The structural difference of the $[011]_C$ poled samples from that of $[001]_C$ or $[111]_C$ poled ones has been delineated.

In our study, a PMN-0.33PT single crystal, with the composition in the MPB region, was chosen as the subject. Domain configurations of this crystal were determined by the polarizing light microscopy (PLM), and the corresponding phase structures **were** inferred based on the extinction position of the **domains** and the orientation of the domain walls. Our intention is to clarify the phase structure of the crystal before poling, and to reveal the dynamic process of polarization rotation and phase transition behavior under an E -field along $[011]_C$. The phase transition sequence with temperature was also one of the main subjects of **this work**.

II. EXPERIMENTAL PROCEDURE

The PMN-0.33PT single crystal (TRS technologies Inc, USA) was grown by the modified Bridgman method. The crystal was oriented by an X-ray diffraction method. Thin sample plates ($\sim 100 \mu\text{m}$) with their large **surfaces** oriented in $[001]_c$ were prepared. The two large surfaces were fine polished for domain observations, then the samples were annealed at 600°C for 1 hour to eliminate the stresses induced by cutting and polishing. A thicker sample, with the dimensions of $1.5 \text{ mm} // [011]_C \times 3 \text{ mm} // [0\bar{1}1]_C \times 0.8 \text{ mm} // [100]_C$ was used for study the dynamic process of domain configurations under changing E -field and temperature. Gold film was vacuum sputtered on the $[011]_C$ and $[0\bar{1}1]_C$ surfaces as electrodes. The domain evolution of structures was observed by a PLM (Zessi Axiokop40) with a crossed

polarizer/analyzer (P/A) pairs. The experimental configuration for the observation of the dynamic process of domains is illustrated in Fig. 1. The E -field was applied along $[011]_C$. For all samples, the optical microscopy observation was performed along $[100]_C$. During the whole observation process, the polarizer was always kept perpendicular to the analyzer.

In order to measure the complete set of dielectric, piezoelectric and elastic constant, several samples were prepared with aspect ratios according to the IEEE standards on piezoelectricity. Combined impedance resonance and pulse-echo ultrasonic method was used to determine the complete set of material constants. Details of the sample preparation and measurement procedure can be found in Refs. [21] and [22].

III. OPTICAL MICROSCOPY STUDIES ON DOMAIN STRUCTURES

The observation of domain configurations using polarizing light microscopy (PLM) is based on the birefringence of the crystal. The high sensitivity of the polarized light transmission intensity to the orientation of the optical indicatrix makes optical microscopy a very powerful tool to study the crystal symmetry. **When a single domain crystal is placed between the mutually perpendicular polarizer and analyzer, the transmitted light intensity is given by the formula**

$$I = I_0 \sin^2 2\alpha \sin^2 \frac{\varphi}{2}. \quad (1)$$

In which I_0 is the amplitude of the transmitted light intensity, α is the angle between the polarizer and the projection of optic axis to the plane perpendicular to the **light propagation direction**, φ is the phase difference between the o and e lights formed in the crystal, which can be expressed by

$$\varphi = \frac{360^\circ}{\lambda} (n_1 - n_2)t, \quad (2)$$

where λ is the wavelength of the light in vacuum, t is the thickness of the crystal and $(n_1 - n_2)$ is the planobirefringence. For a given sample, the thickness t is a

fixed value, resulting in the fixed phase difference φ , hence, the transmitted light intensity depends only on the angle α . When $\alpha = 45^\circ$, the transmitted intensity show maximum value, while at $\alpha = 0^\circ$ or 90° , the intensity is 0, corresponding to the condition of complete extinction.

In most of cases, the sample may contain several layers of domains with different orientations of the optical indicatrix. For a sample with pure **R** or **T** phase, the multidomain layers will only affect the intensity value of the birefringence but not the extinction angle, because the possible angles between the projections of the optical indicatrix axes are 0° or 90° . However, for the monoclinic phase, the angle between projections of optical indicatrix axes of different monoclinic phase layers may take any value, so the crystal may not show extinction at all.

If the crystal is not in a single phase state, i.e., when two or more phases coexist in the crystal, the situation will be more complicated. Here we consider the stacking of one R domain layer and one T domain layer to illustrate the situation. We assume that the intensity and amplitude of the incident light on the sample are I_0 and A , respectively, and the angle between the polarizer and projection of the R domain optical axis is α . After passing through the R domain layer, the phase angle difference between o and e lights is

$$\varphi_1 = \frac{360^\circ}{\lambda} (n_{1R} - n_{2R}) t_R, \quad (3)$$

in which $(n_{1R} - n_{2R})$ is the planobirefringence of R phase and t_R is the thickness of the R domain layer. The angle between the projections of R and T optical axes is 45° . Considering the phase difference, after through the T domain layer, the amplitudes of e and o lights are

$$A_{eT} = \sqrt{\frac{1}{2} A^2 (1 - \sin 2\alpha \cos \varphi_1)}, \quad (4)$$

$$A_{oT} = \sqrt{\frac{1}{2} A^2 (1 + \sin 2\alpha \cos \varphi_1)}, \quad (5)$$

and the phase difference formed in the T phase is

$$\varphi_2 = \frac{360^\circ}{\lambda} (n_{1T} - n_{2T}) t_T, \quad (6)$$

where $(n_{1T} - n_{2T})$ is the planobirefringence of the T phase and t_T is the thickness of the T domain layer. After light going through the analyzer, only the parallel component of $\overline{A_{eT}}$ and $\overline{A_{oT}}$ can be preserved. The phase difference between the o and e light beams is $\varphi_2 + 180^\circ$ when $\alpha < 45^\circ$ and φ_2 when $\alpha > 45^\circ$, so that the intensity through the analyzer is given by

$$I' = \begin{cases} \frac{1}{2} I_0 [(1 - \sin^2 2\alpha \cos \varphi_1) - \cos 2\alpha \sqrt{1 - \sin^2 2\alpha \cos^2 \varphi_1} \cos \varphi_2] & (0 < \alpha \leq 45^\circ) \\ \frac{1}{2} I_0 [(1 - \sin^2 2\alpha \cos \varphi_1) + \cos 2\alpha \sqrt{1 - \sin^2 2\alpha \cos^2 \varphi_1} \cos \varphi_2] & (45^\circ < \alpha \leq 90^\circ) \end{cases} \quad (7)$$

The transmitted intensity depends on both φ_1 and φ_2 . The intensity as a function of α is shown in Fig. 2. At fixed φ_1 and φ_2 , complete extinction may not be obtained for α from 0° to 90° . But $\alpha = 0^\circ$ and $\alpha = 45^\circ$ are always the extreme points. In most cases, the maximum or minimum intensity can be obtained either at 45° or $0^\circ/90^\circ$. Taking KNN-based single crystal in orthorhombic phase as an example, the intensity minimum (but not complete extinction) can be observed when the projections of optical axes of two domain layers form a 45° angle [23].

IV. PHASE STRUCRUE AND DOMAIN CONFIGURATIONS BEFORE POLING

As mentioned above, PMN-0.33PT has the MPB composition. According to previous reports, the crystal could be in the **R**, **T** or **M** phases, or there might be coexistence of two or three of these phases. Before studying the phase transition behavior induced by E -field and temperature, it is important to know the crystal structure and the orientation of spontaneous polarizations (P_s) of the annealed sample.

By using the PLM, important information can be obtained from the optical

extinction positions. For crystals in the ferroelectric R phase, there are 8 possible P_S along $\langle 111 \rangle_C$ family. The projections of P_S on $(100)_C$ surface are along $\langle 011 \rangle_C$ directions. For crystals in the ferroelectric T phase, there are 6 possible P_S along $\langle 001 \rangle_C$ family, and their projections on $(100)_C$ are also in the $\langle 001 \rangle_C$ family [7,23,24]. In our investigation, the angle between the polarizer and $[010]_C$ direction was defined as θ . When observing the $(100)_C$ surface, the R domains show extinction at $\theta=45^\circ$, while the T domains show extinction at $\theta=0^\circ$ (for T domains with P_S along $[001]_C$, $[010]_C$, $[0\bar{1}0]_C$ and $[00\bar{1}]_C$) or omnidirectional extinction (for domains with P_S along $[100]_C$ and $[\bar{1}00]_C$). **Domains that show** extinction at an angle different from 0° , 45° and 90° must belong to the monoclinic phase.

A. Phase structure and polarization direction

In order to reduce the overlap of domains along the observing direction, the platelet sample was thinned down to $100 \mu\text{m}$. As shown in Fig. 3, the platelet sample has three different regions [denoted by A, B and C in Fig. 3]. The A and B regions show extinction at 45° and 50° , respectively, while the C region does not show complete extinction as θ changes from 0° to 180° . The B region should be in monoclinic phase, but it is difficult to discern whether it is M_A with the symmetry of Cm or M_C with the symmetry of Pm . For the A region, there are two possibilities, either R phase or monoclinic M_A phase.

The P_S of M_A phase is confined to the $\{110\}_C$ plane, and there are 24 possible P_S directions. We only illustrated 12 of them in Fig. 4 (a), denoted as P_S #1, #2, ..., #12. The other 12 polarization directions are opposite to these 12 directions. The projections of these 24 polarizations on the $(100)_C$ plane are shown in Fig. 4 (b). The M_A domain with P_S #9, #10, #11, #12 and their opposite counterparts should show extinction at $\theta = 45^\circ$. From Fig. 3, we can see that the A region possesses a volume fraction of more than $1/3$ of the whole sample. We also checked the extinction positions of other samples and found that the volume fractions of the A region, which show extinction at 45° , are always the largest.

In order to figure out if this region belongs to the R phase or M_A phase, let's first consider the dielectric and piezoelectric properties of these two possible phases. When the poling is along $[011]_C$, the R phase would form a “2R” engineered domain pattern with large effective longitudinal piezoelectric d_{33} and dielectric constant ϵ_{33}^T . However, the d_{33} and ϵ_{33}^T values for the $[011]_C$ poled M_A phase should be much smaller because its polarizations are nearly parallel to the E -field after poling. Table I lists the dielectric and piezoelectric constants for the $[011]_C$ poled PMN-0.33PT, and compared with that of the PT-based relaxor single crystals with “2R” engineered domain structure. It can be seen from Table I that the longitudinal piezoelectric and dielectric properties of PMN-0.33PT are much lower than that of the “2R” domain engineered crystals, but the shear piezoelectric constant d_{24} and transverse dielectric constant ϵ_{22}^T are much higher than that of the “2R” domain engineered crystals. For a sample containing a large volume fraction of the R phase, the longitudinal piezoelectric and dielectric properties should be much higher. So the A region must belong to the M_A phase, not the R phase. It can be inferred that the B region should also be in the M_A phase, not in the M_C phase. Overlapping of different M_A domains could not show complete extinction at any position, corresponding to the C region in Fig. 3. Combined the domain configuration and the electrical properties, it can be concluded that the dominant phase of the PMN-0.33PT at room temperature is the M_A phase.

From Fig. 4(b) it can be inferred that the M_A domain with P_S #1 and P_S #2 and their opposite counterparts should show extinction between $\theta=45^\circ$ and 90° , depending on the direction of the polarization. The region B in Fig. 3, which shows extinction at 50° , should correspond to these polarizations. According to the geometrical relationship between P_S and its projection on the $(100)_C$ surface, P_O (shown in Fig. 5), it can be concluded that when P_O is canted 40° from $[001]_C$ (50° from $[010]_C$), P_S should be 49.9° away from $[001]_C$ in the $(\bar{1}10)_C$ plane, and 4.8° away from $[111]_C$, very close to the P_S of the R phase. All polarizations of the M_A phase are confined to

the $\{110\}_C$ planes, however, it is difficult to determine whether all polarizations are 4.8° deviated from the corresponding $\langle 111 \rangle_C$. In other samples, we also observed regions showing extinction angle slightly deviated from 50° , e.g., 51° or 49° , corresponding slight variations of the P_S directions caused by local internal stress and internal bias.

In order to understand domain patterns in a bulk sample, the domain structure of a much thicker sample (0.8 mm) was also observed by the PLM, and the results are shown in Fig. 6. As θ varies from 0° to 90° , no extinction was observed on this sample, this further confirmed that the dominant phase is not the R or T phase, but the M_A phase. In part of the sample, the transmitted light intensity reached the minimum at around $\theta = 20^\circ$, as shown in Fig. 6(b), while in the rest of the sample, the intensity of transmitted light has practically no change with the variation of θ .

B. Formation of domain walls

From Fig. 6, it can be seen on the $(100)_C$ surface that most domain walls are along $[001]_C$. Generally speaking, there might be both charged and uncharged domain walls in PMN-PT single crystal, and both types of domain walls have the same elastic energy. In a well-grown PMN-PT single crystal, the amount of defects and space charges are very low, resulting in low content of charged domain walls. Hence, we only consider the uncharged domain walls below. Sapriel had calculated the permissible domain walls in ferroelectric crystals by mechanical compatibility arguments [27]. Based on his calculations, it can be inferred that the domain wall along $[001]_C$ on the $(100)_C$ surface is permissible [26-28]. For example, the W_f domain wall formed between P_S #5 and P_S #8, and between P_S #6 and P_S #7 are all along $[001]_C$. The diagrammatic sketch of a W_f domain wall between P_S #5 and P_S #8 is shown in Fig. 7(a). Also, S domain walls formed between P_S #5 and P_S #6, and between P_S #6 and P_S #7 are along $[001]_C$, as shown in Fig. 7(b). There are also other W_f or S domain walls between different polarizations along $[001]_C$, and they all follow the same principle.

C. Possibility of other coexisting phases

As mentioned above, the bulk sample does not show extinction at 0° or 45° . However, from this fact alone we cannot completely exclude the existence of R and T phases. If small R or T domain blocks stacking with several M_A domain layers vertically, it may not show extinction at all. What we can say is that if R or T domains exist, their size and total volume ratio must be very small. From the experimental results, we can conclude that the dominant phase of PMN-0.33PT at room temperature is the M_A phase before poling.

V. E -FIELD DEPENDENT DOMAIN CONFIGURATIONS AND PHASE TRANSITIONS

A. Phase transitions under E -field along $[011]_C$

The domain structure evolution was observed at room temperature by applying a dc E -field along $[011]_C$. As shown in Fig. 8, before the application of the E -field [Fig. 8 (a)], the dominant phase is M_A with 24 possible polarization variants. As the E -field increases, the domain structure showed little change until $E = 1.8$ kV/cm, at which the whole sample becomes dark (Fig. 8(b)), indicating that the polarizations have been switched to directions closer to the E -field direction. At the same time, the original $[001]_C$ domain walls disappeared while $[010]_C$ domain walls emerged. Considering that the polarizations should be relatively close to $[011]_C$, these domain walls are between $P_S \#2$ and $P_S \#4$, $P_S \#1$ and $P_S \#3$ (W_f domain wall), or between $P_S \#1$ and $P_S \#4$, $P_S \#2$ and $P_S \#3$ (S domain wall), respectively. As the E -field further increases, the polarizations get even closer to $[011]_C$. The number of $[010]_C$ domain walls decreases gradually. Parts of the sample showed complete extinction, which is associated with the formation of single domain orthorhombic (O) phase with P_S along $[011]_C$. **Two kinds of S domain walls**, about 28° away from $[001]_C$ and $[010]_C$, have been observed (**denoted as S_1 and S_2 , respectively**), as shown in Fig. 8(c). The inset of Fig. 8(c) is an enlarged view of **S_1 and S_2** domain walls. The S_1 domain wall was formed between $P_S \#5$ and $P_S \#7$, while S_2 was formed between $P_S \#1$ and $P_S \#2$. Fig. 9 shows the schematic drawings of S_1 and S_2 domain walls. As the E -field is increased

to 2.5 kV/cm, **part** of the M_A phase transformed into the O phase, while rest of the crystal are still in the M_A phase, now **with only 4 polarizations that are closest to $[011]_C$ (i.e., P_S #1, #2, #5 and #7)**. Interestingly, the domain structure of a small region (top right in Fig.8(c)) in the sample is much different from the rest. The intensity of the transmitted light reaches the maximum at $\theta=45^\circ$ and the minimum at $\theta=0^\circ$, but complete extinction cannot be obtained, as shown in the inset (bottom left of Fig.8(c)). Due to the overlapping of different domains, it is difficult to determine the phase structure of this region. However, it cannot be the R phase because it shows the same extinction position as the O phase domains with P_S along $[011]_C$. We **think** this region is in the T phase. According to Eq. (7) and Fig. 2, when the angle between the projections of the two optical axes is 45° , the transmitted light intensity becomes the maximum at $\theta=45^\circ$ ($\alpha=0^\circ$) and minimum at $\theta=0^\circ$ ($\alpha=45^\circ$). An E -field along $[011]_C$ cannot induce the T phase, so it must be inherited from the unpoled state. In other words, the unpoled sample is dominantly in the M_A phase, which coexists with a small volume fraction of the T phase. As the E -field further increases to 6 kV/cm, the whole sample shows optical extinction at 45° [Fig. 8(d)] and light transmission at 0° [inset of Fig. 8(d)], indicating that the sample is in single domain O phase with P_S along $[011]_C$. Fig. 8(e) and (f) show domain structures as the E -field decreases to $E=2$ kV/cm and $E=0$ kV/cm, respectively. Generally speaking, the single domain O phase can be maintained after the E -field is removed.

One may wonder if the monoclinic M_C phase could be formed during the phase transition process from the M_A to O phase, since its polarization is much closer to that of the O phase. The polarizations of the M_C phase are confined to the $\{001\}_C$ planes, as shown in Fig. 10(a), in which we give only 12 of the 24 possible P_S [13]. Under an electric field along $[011]_C$, the polarizations would switch to P_S #1 and P_S #5 positions, which are the closest to $[011]_C$. The domain wall between P_S #1 and P_S #5 is a W_f domain wall, which is along $[0\bar{1}1]_C$ when observed on the $(100)_C$ surface, as shown in Fig. 10(b) [26,27]. Since no domain wall along this direction was observed during the E -field induced phase transition process, we can conclude that the phase

transition sequence under the $[011]_C$ E -field is directly from M_A to O , no intermediate M_C phase has been formed.

B. Polarization rotation under E -field

In order to understand the origin of high piezoelectricity in the MPB composition, it is important to investigate the rotation path of P_S under an E -field. As can be seen in Fig. 9, the intersection of S_1 domain wall and $(100)_C$ surface should be perpendicular to the projection of P_S #5 (or P_S #7). Correspondingly, the intersection of S_2 domain wall should be perpendicular to the projection of P_S #1 (or P_S #2). If P_S is allowed to rotate continuously in the $\{011\}_C$ planes, the S domain wall will also be allowed to change continuously. So we should pay special attention to the directions of S_1 and S_2 domain walls, based on their orientations the orientation of P_S can be calculated. In Fig. 8 (c), S_1 and S_2 domain walls are about 28° away from the $[001]_C$ and $[010]_C$ directions. This means that the projections of P_S #1 and P_S #2, which forms the S_2 that is 28° away from $[001]_C$; and the projections of P_S #5 and P_S #7, which forms S_1 that is 28° away from $[010]_C$. According to Fig. 5, the corresponding P_S is calculated to be 17.8° deviated from the nearest $\langle 111 \rangle_C$. This value is very different from the P_S direction (about 4.8° away from $\langle 111 \rangle_C$) in the unpoled samples. The results confirmed that the orientation of P_S changed a lot under an E -field.

To investigate the rotation behavior of P_S #1, #2, 5# and #7 under an E -field, variations of S_1 and S_2 domain walls with the increasing E -field are observed using much larger magnification. Fig. 11 (a) shows that both S_1 and S_2 domain walls exist. Three kinds of S_1 domain walls have been found with different orientations, e.g., 18° , 22° and 30° away from $[001]_C$, and the corresponding P_S #5 and P_S #7 are calculated to be 30.1° , 25.0° and 15.5° deviated from the nearest $\langle 111 \rangle_C$, respectively. The allowed S_2 domain wall directions are much limited, most S_2 domain walls are oriented about 26° away from $[010]_C$, which means that the corresponding P_S is 20.1° away from $\langle 111 \rangle_C$. With the increase of the E -field, S_1 domain walls gradually disappear and continuous rotation of the S domain walls was not observed. When the E -field is increased to 4 kV/cm, only S_2 domain walls can be observed as shown in

Fig. 11(b). This means that polarizations (P_S #5 and P_S #7) forming the S_1 domain walls have been switched to $[011]_C$ direction through a field induced phase transition. Our results indicate that the polarization rotation from the original M_A phase to the final O phase is through a discontinuous jump.

In summary, P_S of M_A phase in the unpoled sample is very close to that of the R phase (only 4.8° away from $\langle 111 \rangle_C$). This position should be stable with a minimum energy before the application of the E -field. Under a large E -field along $[011]_C$, only four P_S closest to $[011]_C$ will be preserved, e.g., P_S #1, P_S #2, P_S #5 and P_S #7, and the original energy profile will be changed. Under the combined effect of an E -field and internal stresses, P_S will be rotated to a direction further away from $\langle 111 \rangle_C$ to achieve a new energetically stable state. When the E -field is increased to 6 kV/cm, P_S will overcome the potential barrier and be switched to $[011]_C$, i.e., a field induced phase transition occurred from the M_A phase to O phase.

For a ferroelectric solid solution system, like PMN-PT and PZT systems, when the composition is near the MPB, there will be co-existence of R and T phases. Due to the mismatch of lattice structures between R and T phases, both crystal structures have to distort in order to accommodate each and to maintain the atomic coherency at the interface. This local interface strain is present even without external fields. Such local strains have influence on the stability of both R and T phases. As a result of the distortions caused by the strain mismatch at the interface, an adaptive monoclinic phase is formed [29]. Our recent work based on the Landau-Devonshire phenomenology had confirmed theoretically that the internal strains can influence the potential wells, and a monoclinic phase could be induced due to the strain mismatch between the R and T phases [30]. The free energy profile near the MPB is rather flat along a slim and shallow path, so that very small stimuli could produce relatively large polarization rotation along the path, producing very large dielectric and piezoelectric effects [31].

C. Stability of the induced single domain O phase

Usually the single domain state is unstable due to high internal stresses [32]. We

have studied the stability of the induced single domain O phase for different aging time. Fig. 12 shows the domain configurations of PMN-0.33PT after a certain time of aging. Shortly after the removal of the E -field, less-opaque areas can be observed (upper right and lower right in Fig. 12(a)). With the increase of aging time, the transmission region becomes larger, and the intensity of transmitted light becomes stronger. Meanwhile, S_1 and S_2 domain walls start to appear. The domain structure shows the coexistence of M_A (with only 4 possible P_S , #1, #2, #5 and #7) and the O phase (with P_S along $[011]_C$). However, it is difficult to determine the volume fractions of the two phases from these images. Generally, the volume fraction of the M_A phase would increase while that of the O phase would decrease with aging time.

D. Full tensor properties of $[011]_C$ poled quasi single domain PMN-0.33PT crystal

In order to learn the macroscopic performance of PMN-0.33PT single crystal, the complete set of the elastic, piezoelectric and dielectric constant for $[011]_C$ poled quasi single domain PMN-0.33PT single crystal are measured. All measured samples are poled under an E -field of 10 kV/cm, so that single domain O phase can be achieved through poling. All measurements were carried out 24 h after poling, hence the actual phase structure for these samples should be the coexistence of M_A and O phase. The measured data are listed in Table II. The crystal exhibits high transverse dielectric constant $\epsilon_{22}^T=16816$ and $\epsilon_{11}^T=5197$, but low longitudinal dielectric constant $\epsilon_{33}^T=816$. On the other hand, the thickness shear mode piezoelectric coefficient d_{15} and d_{24} are all more than 10 times higher than that of the longitude mode ($d_{33}=165$ pC/N). Although the samples are not pure single domain O phase, the full tensor properties are much like that of a single domain structure with strong anisotropy. This confirms the fact that after 24 h aging, the single domain O phase is still the dominant phase in $[011]_C$ poled PMN-0.33PT.

VI. PHASE TRANSITION SEQUENCE AND DOMAIN CONFIGURATION EVOLUTION WITH TEMPERATURE

A. Phase transition sequence during heating process

After 24 h of aging, the domain structure of $[011]_C$ poled PMN-0.33PT single crystal was studied as a function of temperature. As shown in Fig. 13, at room temperature, the phase structure is the mixture of M_A and O phases [Fig. 13(a)]. With the increase of temperature, the sample gradually became less transparent at $\theta=45^\circ$ [Fig. 13(b)]. At 55°C , the sample showed complete extinction at $\theta=45^\circ$ and transparent at $\theta=0^\circ$ [Fig. 13(c) and (d)]. Two kinds of domain configurations may explain this optical behaviors: single domain O phase with P_S along $[011]_C$, or R phase. The single domain O phase should be excluded due to its instability at higher temperatures; hence, the phase structure at 55°C should belong to the R phase. The R phase is maintained upon further heating until 93°C , at which R domains disintegrated dramatically and a new phase emerged. The inset of Fig. 13(e) shows the domain image during this phase transition process, Fig. 13 (e) and (f) show the domain structures of the new phase at $\theta=45^\circ$ and 0° , respectively. Generally speaking, with the increase of temperature, the R phase is usually transformed into the T phase in the MPB composition of the solid solution [32]. However, in our investigation, the new phase did not show complete extinction as θ varies from 0° to 90° , which is inconsistent with the optical behavior of the T phase but more like the M phase. Most of domain walls in the new phase are along $[0\bar{1}1]_C$.

Now, let us consider the situation of the M_C phase. For the $[011]_C$ poled sample, $P_S \#1$ and $P_S \#5$ in the M_C phase are preferred, as can be seen in Fig. 10(a). The uncharged domain wall formed between $P_S \#1$ and $P_S \#5$ is along $[0\bar{1}1]_C$ (Fig. 10(b)), consistent with the domain wall direction shown in Fig. 13 (e). Also, in a M_C phase with most polarizations along $P_S \#1$ and $P_S \#5$, no extinction position should be observed due to the overlap of different domain layers. When the temperature is further increased to 155°C , another dramatic change of domain structures was observed (Fig. 13(g) and (h)). The inset of Fig. 13 (g) shows the domain configuration during the phase transition process. The new phase shows extinction for all θ from 0°

to 90° , indicating the formation of the cubic (C) phase. However, a small fraction of the R phase nanodomain clusters is still embedded in the cubic phase, result in the incomplete extinction at $\theta=0^\circ$ [Fig. 13 (h)]. As the temperate further increases, the remaining R phase cluster gradually changed into C phase, as shown in Fig. 13 (i) and (j).

In summary, with the increase of temperature, the phase transformation sequence of the $[011]_C$ poled PMN-0.33PT is as follows: coexistence of M_A and O phase \rightarrow R phase $\rightarrow M_C$ phase \rightarrow cubic (C) phase. *Tu et al* has studied the temperature induced phase transition of $[111]_C$ orientated PMN-0.33PT single crystals. It was reported that the $[111]_C$ orientated crystal disfavors the tetragonal phase and persists in the monoclinic phase up to 420 K (147 °C), at which the cubic phase was formed [33]. Moreover, in the $[001]_C$ poled PMN-PT single crystals, the T phase is unavoidable before the formation of the C phase in the heating process [10,34,35]. Based on the above information, it can be concluded that the poling direction greatly affects the phase transition behavior. When poling the crystal along different directions, different internal *E*-bias and internal stresses (both in direction and magnitude) will be formed, which play an important role in regulating the phase transition sequence. This phenomenon is particularly evident for the MPB composition due to the fact that the amplitude and orientation of P_S is very sensitive to *E*-bias and stresses.

B. Phase transition sequence during cooling process

The phase transition behavior of PMN-0.33PT was further studied with the decrease of temperature. The PLM images are shown in Fig. 14. It can be seen that the sample shows C phase above 141 °C [Fig. 14(a) and (b)]. Dramatic domain changes occur at 141 °C [Fig. 14(c) and (d)]. The new phase should be the T phase, which show extinction at $\theta=0^\circ$ and transparency at $\theta=45^\circ$. The T phase **persisted** in the temperature range of 141 °C \sim 68 °C. At 68 °C, another phase transition **was** observed, accompanied by an abrupt change in domain structures (Fig. 14(e) and (f)). There is no more phase change down to room temperature (Fig. 14(g) and (h)). In this new phase, domain walls are along $[001]_C$. Parts of the sample show intensity

minimum around $\theta=20^\circ$ [inset of Fig. 14(h)], coincides with the domain patterns of the unpoled sample, which is in the M_A phase. The phase transition sequence during cooling process is therefore as follows: C phase \rightarrow T phase \rightarrow M_A phase. Here, the phase transition sequence during cooling is independent of crystallographic orientation due to the starting unique paraelectric phase at temperatures above T_C .

The hysteretic phase transition sequence of the PMN-0.33PT during heating and poling process is summarized in Fig. 15. Starting from the upper left of the figure at room temperature, the $[011]_C$ poled crystal is primarily in the O phase with a small portion of M_A phase. As the crystal is heated, it will go through the phase transition from the M_A phase to the R phase at 55°C , then to the M_C phase at 93°C and finally to the C phase at 155°C . On cooling, the crystal will be transformed to the T phase at 141°C and the M_A phase at 68°C .

VII. SUMMARY AND CONCLUSIONS

In conclusion, we have intensively studied the phase structures of MPB composition PMN-0.33PT single crystal by PLM. The E -field and temperature induced phase transition sequences were also investigated. Based on our results, we may draw the following conclusions:

(i) At room temperature, the dominant phase of unpoled PMN-0.33PT single crystal is the M_A phase. The polarizations of M_A phase are estimated to be around 4.8° deviation from the corresponding $\langle 111 \rangle_C$ directions in the $\{011\}_C$ planes. A small fraction of the T phase also exists.

(ii) Application of a large enough E -field along $[011]_C$ can induce the M_A -O phase transition. A single domain O phase with polarization along $[011]_C$ can be obtained under a dc bias of 6 kV/cm. The induced single domain O phase is not entirely stable. After the removal of the dc bias, part of the O phase gradually returns back to the M_A phase, but the dominant volume fraction is still in the O phase.

(iii) The complete set of dielectric, piezoelectric and elastic constants of $[011]_C$ poled PMN-0.33PT has been determined, which shows strong anisotropy with

orthorhombic macroscopic symmetry. Hence the crystal may be treated as single domain O phase.

(iv) The phase transition sequence of the $[011]_C$ poled PMN-0.33PT single crystal shows a strong hysteretic feature. During the heating process, the sequence is $M_A \rightarrow R \rightarrow M_C \rightarrow C$, much different from that of the $[001]_C$ poled PMN-PT single crystals. So the transition sequence is poling direction dependent. While on cooling, the transition sequence is $C \rightarrow T \rightarrow M_A$, which is independent of the crystal orientation.

These interesting findings shed some light on the coexisting phases in the MPB composition PMN-PT single crystals, and provide a clear picture on the hysteretic nature of the temperature induced phase transition sequence.

ACKNOWLEDGEMENTS

This work was supported by the National Key Basic Research Program of China (No. 2013CB632900), the NIH under Grant No. P41-EB21820, the National Science Foundation of China (Nos. 51102062, 11372002, 51302056, and 51472197), and the Postdoctoral Foundation of Heilongjiang Province (No. LBH-Z10147).

Reference

- [1] E. Sun, and W. Cao, *Prog. Mater. Sci.* **65**, 124 (2014).
- [2] S. Zhang, and F. Li, *J. Appl. Phys.* **111**, 031301 (2012).
- [3] C. Okawara, and A. Amin, *Appl. Phys. Lett.* **95**, 072902 (2009).
- [4] T. Wu, P. Zhao, M. Bao, A. Bur, J. L. Hockel, K. Wong, K. P. Mohanchandra, C. S. Lynch, and G. P. Carman, *J. Appl. Phys.* **109**, 124101 (2011).
- [5] T. R. Shrout, Z. P. Chang, N. Kim, and S. Markgraf, *Ferroelectrics Lett.* **12**, 63 (1990).
- [6] A. K. Singh, and D. Pandey, *Phys. Rev. B* **67**, 064102 (2003).
- [7] R. Kandilian, A. Navid, and L. Pilon, *Smart Mater. and Struct.* **20**, 055020 (2011).
- [8] M. Ahart, M. Somayazulu, R. Cohen, P. Ganesh, P. Dera, H.-k. Mao, R. J. Hemley, Y. Ren, P. Liermann, and Z. Wu, *Nature* **451**, 545 (2008).
- [9] F. Bai, N. Wang, J. Li, D. Viehland, P. Gehring, G. Xu, and G. Shirane, *J. Appl. Phys.* **96**, 1620 (2004).
- [10] D. Lin, Z. Li, S. Zhang, Z. Xu, and X. Yao, *J. Appl. Phys.* **108**, 034112 (2010).
- [11] B. Noheda, D. E. Cox, G. Shirane, J. Gao, and Z.-G. Ye, *Phys. Rev. B* **66**, 054104 (2002).
- [12] B. Noheda, D. E. Cox, G. Shirane, J. Gonzalo, L. Cross, and S.-E. Park, *Appl. Phys. Lett.* **74**, 2059 (1999).
- [13] B. Noheda, D. E. Cox, G. Shirane, S.-E. Park, L. Cross, and Z. Zhong, *Phys. Rev. Lett.* **86**, 3891 (2001).
- [14] R. Guo, L. E. Cross, S.-E. Park, B. Noheda, D. E. Cox, and G. Shirane, *Phys. Rev. Lett.* **84**, 5423 (2000).
- [15] R. Chien, V. H. Schmidt, C.-S. Tu, L.-W. Hung, and H. Luo, *Phys. Rev. B* **69**, 172101 (2004).
- [16] Z.-G. Ye, B. Noheda, M. Dong, D. Cox, and G. Shirane, *Phys. Rev. B* **64**, 184114 (2001).

- [17]G. Xu, H. Luo, H. Xu, and Z. Yin, Phys. Rev. B **64**, 020102 (2001).
- [18]Y. Lu, D.-Y. Jeong, Z.-Y. Cheng, Q. Zhang, H.-S. Luo, Z.-W. Yin, and D. Viehland, Appl. Phys. Lett. **78**, 3109-3111 (2001).
- [19]S. Zhang, G. Liu, W. Jiang, J. Luo, W. Cao, and T. R. ShROUT, J. Appl. Phys. **110**, 064108 (2011).
- [20]X. Huo, S. Zhang, G. Liu, R. Zhang, J. Luo, R. Sahul, W. Cao, and T. R. ShROUT, J. Appl. Phys. **112**, 124113 (2012).
- [21] L. Zheng, S. Li, S. Sang, J. Wang, X. Huo, R. Wang, Z. Yuan, and W. Cao, Appl. Phys. Lett. **105**, 212902 (2014).
- [22] R. Zhang, B. Jiang W. Jiang, and W. Cao, Appl. Phys. Lett. **89**, 242908 (2006).
- [23]L. Zheng, J. Wang, X. Huo, R. Wang, S. Sang, S. Li, P. Zheng, and W. Cao, J. Appl. Phys. **116**, 044105 (2014).
- [24]R. Chien, V. H. Schmidt, L.-W. Hung, and C. S. Tu, J. Appl. Phys. **97**, 114112 (2005).
- [25] E. Sun, S. Zhang, J. Luo, T. R. ShROUT, and W. Cao, Appl. Phys. Lett. **97**, 032902 (2010)
- [26]A. Bokov, and Z.-G. Ye, J. Appl. Phys. **95**, 6347 (2004).
- [27]J. Sapriel, Phys. Rev. B **12**, 5128 (1975).
- [28]J. Erhart, Phase Transitions **77**, 989 (2004).
- [29] D. D. Viehland, and E. K. H. Salje, Adv. Phys. **63**, 267 (2014).
- [30] X. Lu, L. Zheng, H. Li, and W. Cao, J. Appl. Phys. **117**, 134101 (2015).
- [31] D. Damjanovic, J. Am. Ceram. Soc. **88**, 2663 (2005).
- [32]R. Zhang, B. Jiang, and W. Cao, Appl. Phys. Lett. **82**, 787 (2003).
- [33]C.-S. Tu, V. H. Schmidt, I.-C. Shih, and R. Chien, Phys. Rev. B **67**, 020102 (2003).
- [34] M. Shen, G. Siu, Z. Xu, and W. Cao, Appl. Phys. Lett. **86**, 252903 (2005).
- [35]Y. Guo, H. Luo, D. Ling, H. Xu, T. He, and Z. Yin, J. Phys.: Condens. Matt. **15**, L77 (2003).

Table I. Property comparison among $[011]_C$ poled PMN-0.33PT and other PT-based relaxor single crystals with “2R” engineered domain configuration.

Material	d_{33} (pC/N)	d_{15} (pC/N)	d_{24} (pC/N)	ϵ_{33}^T	ϵ_{11}^T	ϵ_{22}^T
PMN-0.33PT ^a	165	2321	1941	816	5197	16816
PIN-PMN-0.32PT [25]	1363	3354	162	4361	6814	1483
PZN-0.07PT [22]	1150	1823	50	3180	8240	1865

^a This work.

Table II. Measured and derived material constants of $[011]_C$ poled PMN-0.33PT crystal. (Density: $\rho = 8114 \text{ kg/m}^3$)

Elastic stiffness constants: c_{ij}^E and c_{ij}^D (10^{10} N/m^2)											
c_{11}^E	c_{12}^E	c_{13}^E	c_{22}^E	c_{23}^E	c_{33}^E	c_{44}^E	c_{55}^E	c_{66}^E			
21.2	12.6	7.9	16.4	10.3	15.0	2.8	0.72	7.8			
c_{11}^D	c_{12}^D	c_{13}^D	c_{22}^D	c_{23}^D	c_{33}^D	c_{44}^D	c_{55}^D	c_{66}^D			
22.7	9.3	1.3	17.4	7.4	16.1	9.6	4.6	7.8			
Elastic compliance constants: s_{ij}^E and s_{ij}^D ($10^{-12} \text{ m}^2/\text{N}$)											
s_{11}^E	s_{12}^E	s_{13}^E	s_{22}^E	s_{23}^E	s_{33}^E	s_{44}^E	s_{55}^E	s_{66}^E			
8.7	-7.9	4.5	15.9	-9.0	11.8	35.7	138.9	12.8			
s_{11}^D	s_{12}^D	s_{13}^D	s_{22}^D	s_{23}^D	s_{33}^D	s_{44}^D	s_{55}^D	s_{66}^D			
5.8	-3.6	1.2	9.4	-4.1	8.0	10.4	21.8	12.8			
Piezoelectric coefficients: $d_{i\lambda}$ (10^{-12} C/N), $e_{i\lambda}$ (C/m^2), $g_{i\lambda}$ (10^{-3} Vm/N), $h_{i\lambda}$ (10^8 V/m)											
d_{15}	d_{24}	d_{31}	d_{32}	d_{33}	e_{15}	e_{24}	e_{31}	e_{32}	e_{33}		
2321	1941	143	-216	165	16.7	54.3	7.5	-6.2	6.4		
g_{15}	g_{24}	g_{31}	g_{32}	g_{33}	h_{15}	h_{24}	h_{31}	h_{32}	h_{33}		
50.5	13.0	19.8	-29.9	22.8	23.2	12.5	20.0	-16.6	17.2		
Dielectric constants: ϵ_{ij}^T (ϵ_0) and β_{ij}^S ($10^{-4}/\epsilon_0$)											
ϵ_{11}^T	ϵ_{22}^T	ϵ_{33}^T	ϵ_{11}^S	ϵ_{22}^S	ϵ_{33}^S	β_{11}^T	β_{22}^T	β_{33}^T	β_{11}^S	β_{22}^S	β_{33}^S
5197	16816	816	814	4896	423	1.92	0.59	12.25	12.3	2.04	23.6
Electromechanical coupling factors											
k_{15}	k_{24}	k_{31}	k_{32}	k_{33}	k_t						
0.918	0.842	0.572	0.637	0.567	0.262						

Figure captions:

Fig. 1 The experimental setup for observing domain structures using polarizing light microscopy. A bias field was applied along $[011]_C$, while domain structure observation was on the $(100)_C$ surface.

Fig. 2 The intensity of transmitted light as a function of α . (a) φ_2 is fixed at 45° , φ_1 changes from 0° to 180° , and (b) φ_1 is fixed at 45° , φ_2 changes from 0° to 180° .

Fig. 3 Domain structures of unpoled PMN-0.33PT single crystal. There are three different regions: A, B and C. (a) $\theta=0^\circ$, (b) $\theta=45^\circ$ and (c) $\theta=50^\circ$.

Fig. 4 (a) Schematic drawing of possible P_S states in the M_A phase. (b) Projections of P_S in the M_A phase onto the $(100)_C$ plane.

Fig. 5 Geometrical relationship between P_S (the red arrow) and its projection P_O (the green arrow) on the $(100)_C$ plane. When P_O is 40° away from $[001]_C$ in the $(100)_C$ plane, P_S is 49.9° away from $[001]_C$, and 4.8° away from $[111]_C$ in the $(\bar{1}10)_C$ plane.

Fig. 6 Domain structures at room temperature after annealing. (a) $\theta=45^\circ$, (b) $\theta=20^\circ$.

Fig. 7 Schematic drawings of (a) W_f domain wall between P_S #5 and P_S #8, and (b) S domain wall between P_S #5 and P_S #6.

Fig. 8 E -field dependence of domain structures at room temperature with a dc E -field applied along $[011]_C$. (a) 0 kV/cm; (b) 1.8 kV/cm; (c) 2.5 kV/cm; (d) 6 kV/cm during the field increasing process, and (e) 2.5 kV/cm; (f) 0 kV/cm during the field decreasing process.

Fig. 9 Schematic drawings of (a) S_2 domain wall between P_S #1 and P_S #2, and (b) S_1 domain wall between P_S #5 and P_S #7.

Fig. 10 Schematic drawing of (a) the possible P_S states in the unpoled M_C phase and (b) domain wall between P_S #1 and P_S #5.

Fig. 11 Variation of S domain walls under different E -field. (a) 3 kV/cm; (b) 4 kV/cm.

Fig. 12 Domain structures of $[011]_C$ poled PMN-0.33PT single crystal after an

ageing time of (a) 5 min; (b) 2 h; (c) 8 h and (d) 24 h.

Fig. 13 Domain structures observed at various temperatures during heating process. (a) 30 °C; (b) 40 °C; (c) and (d) 55 °C; (e) and (f) 93 °C; (g) and (h) 153 °C; (i) and (j) 153 °C; (k) and (l) 170 °C. (a), (b), (c), (e), (g) and (i) were taken at $\theta=45^\circ$, while (d), (f), (h) and (j) were taken at $\theta=0^\circ$.

Fig. 14 Domain structures observed at various temperatures during cooling process. (a) and (b) 150°C; (c) and (d) 141 °C; (e) and (f) 68 °C; (g) and (h) 30 °C. The left column corresponds to $\theta=45^\circ$ and the right corresponds to $\theta=0^\circ$.

Fig. 15 Schematic of the hysteretic phase transition sequence during heating and cooling processes (lattice deformation not in real scale).

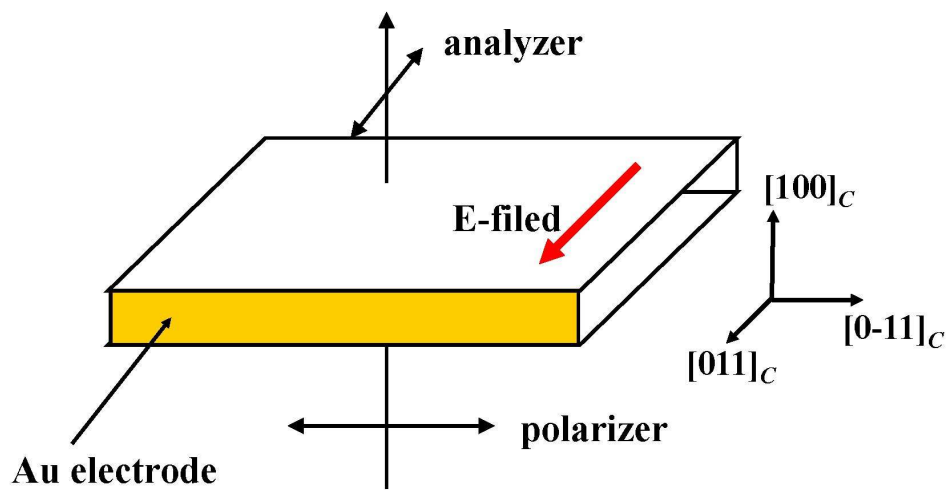


Figure 1 BB12509 12APR15

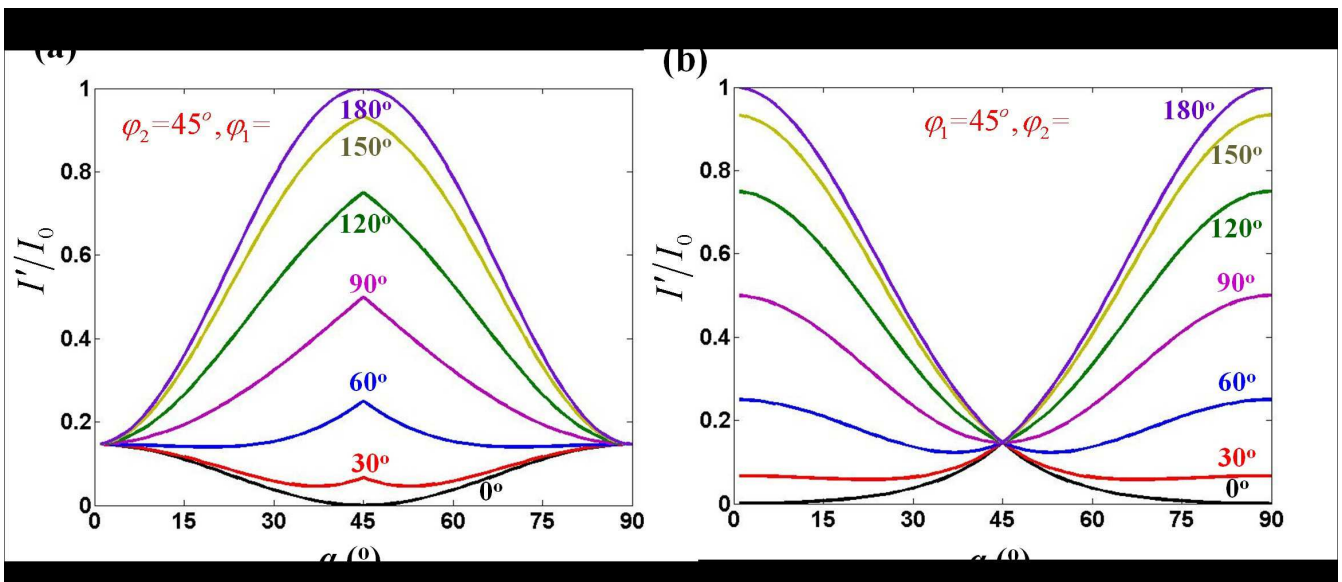


Figure 2

BB12509

12APR15

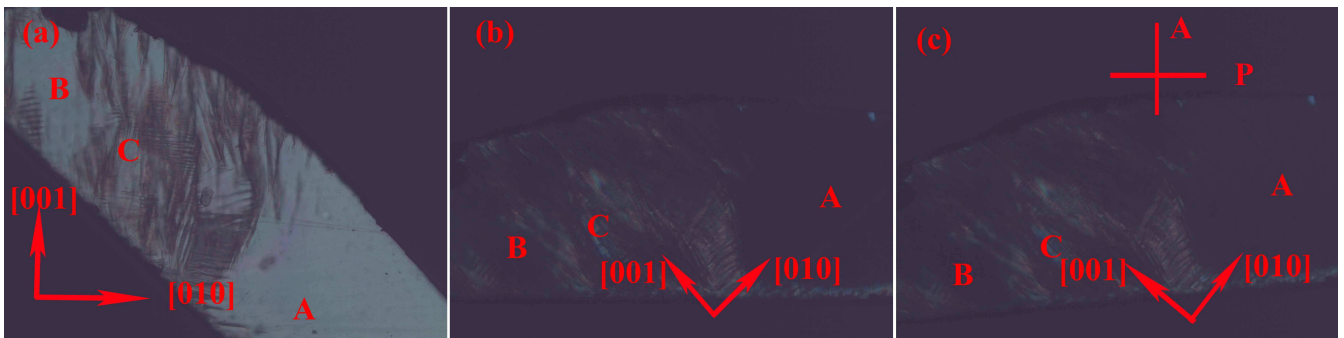


Figure 3

BB12509

12APR15

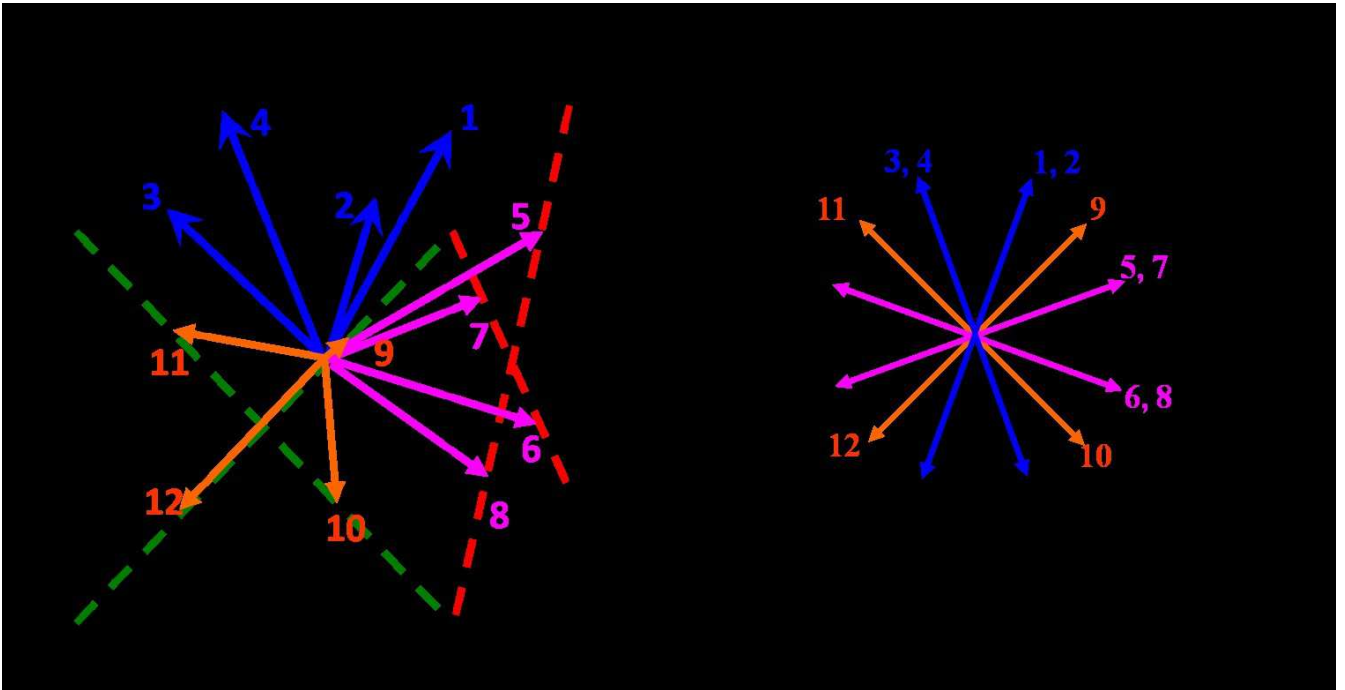


Figure 4

BB12509

12APR15

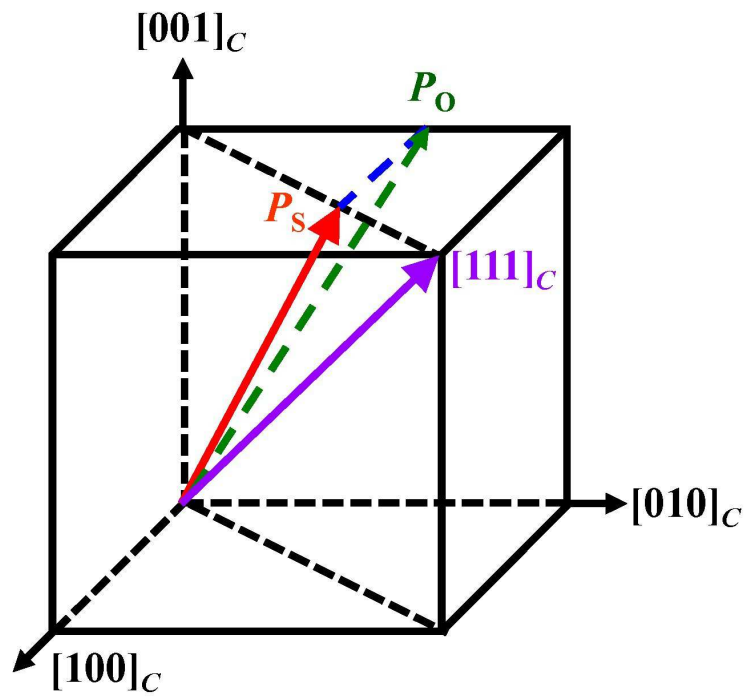


Figure 5

BB12509

12APR15

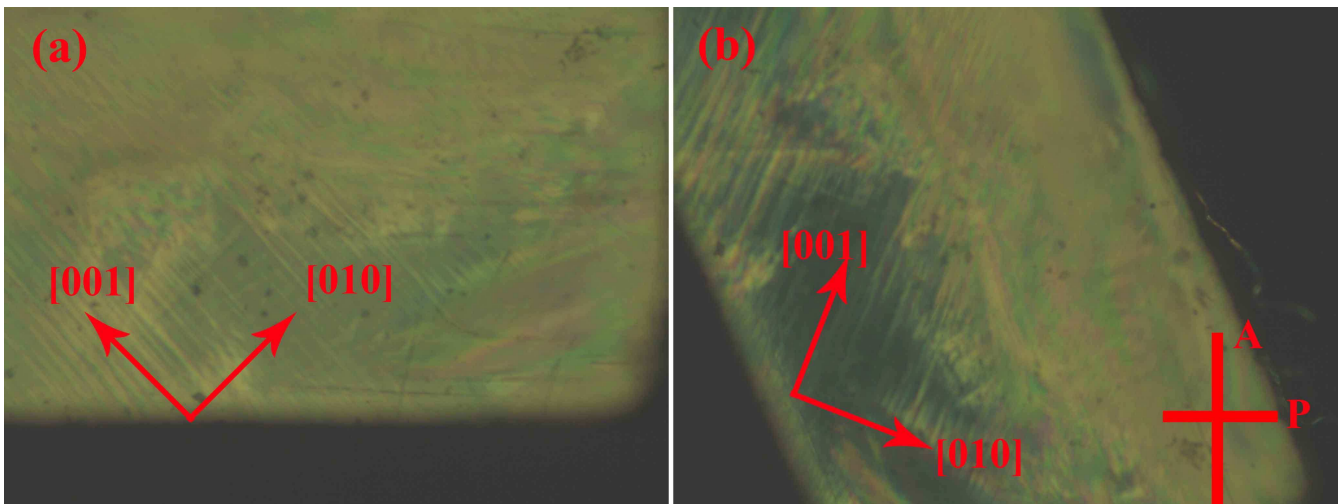


Figure 6

BB12509

12APR15

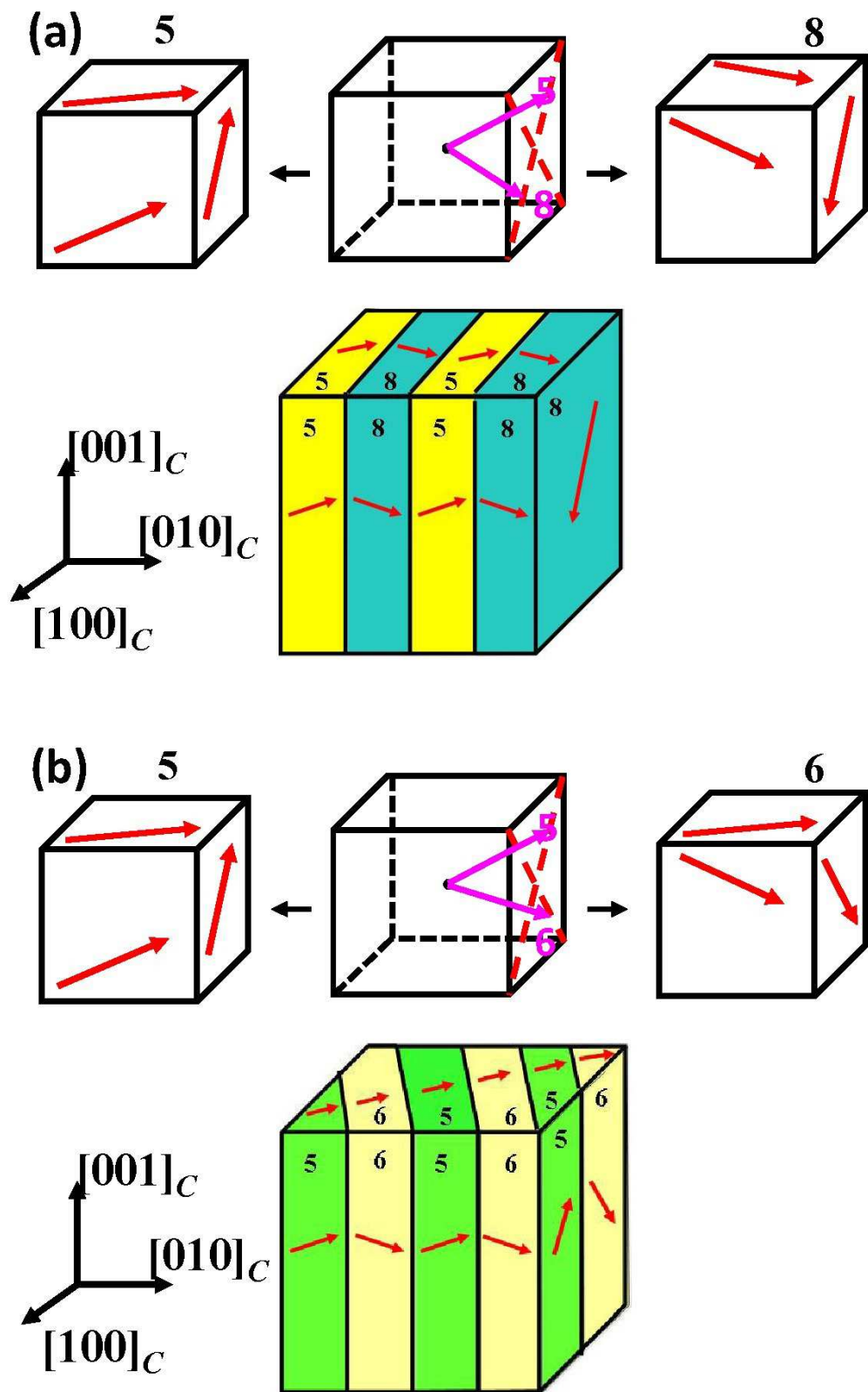


Figure 7

BB12509

12APR15

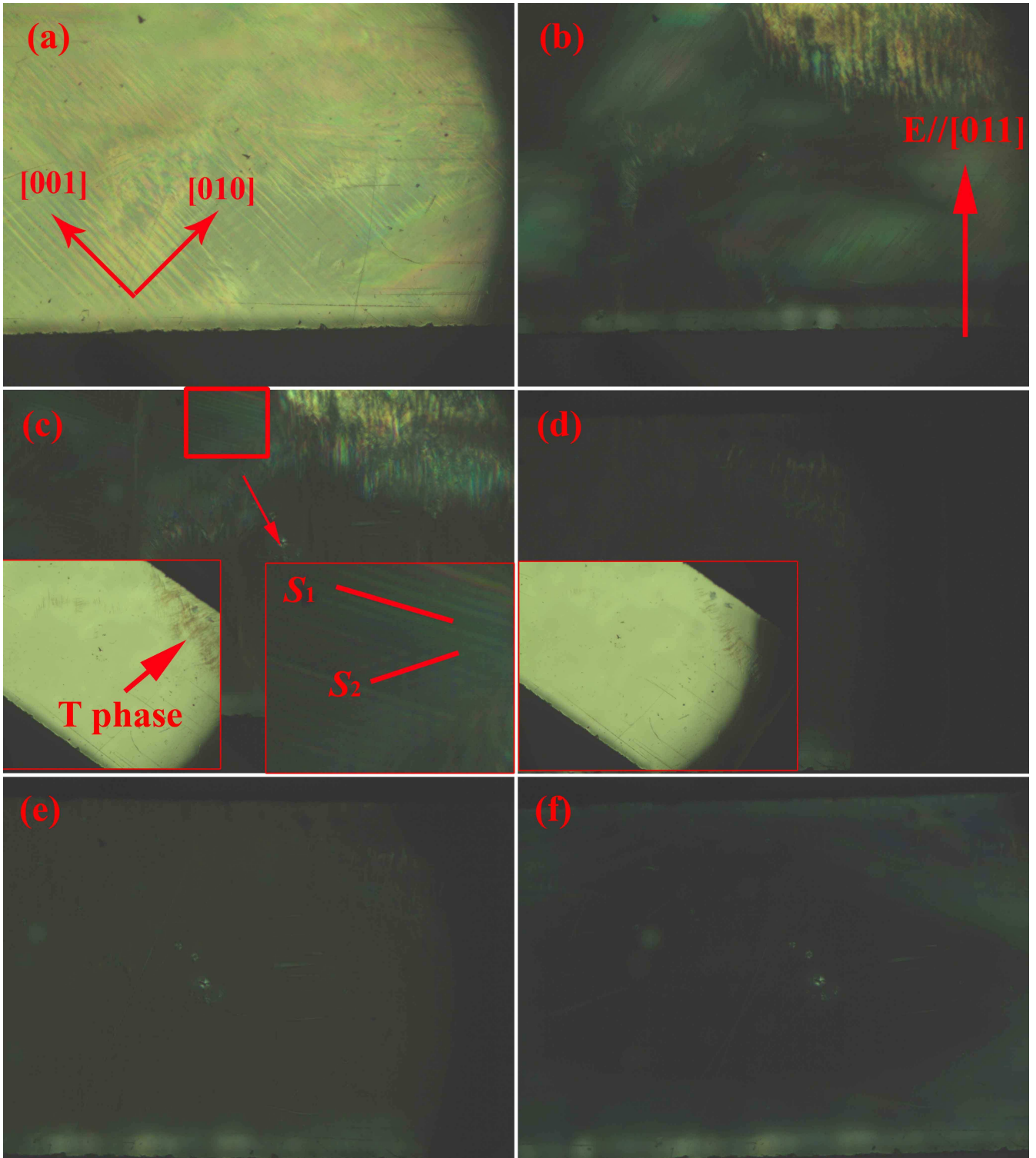


Figure 8

BB12509

12APR15

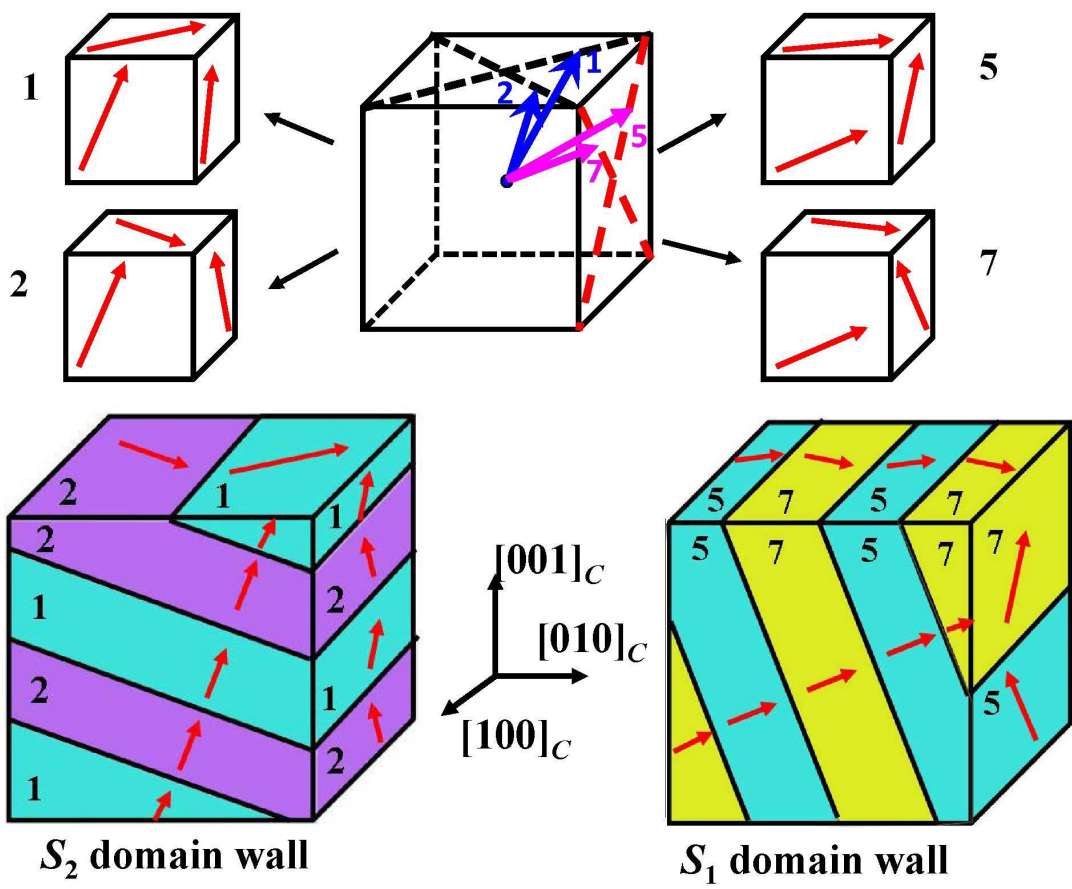


Figure 9

BB12509

12APR15

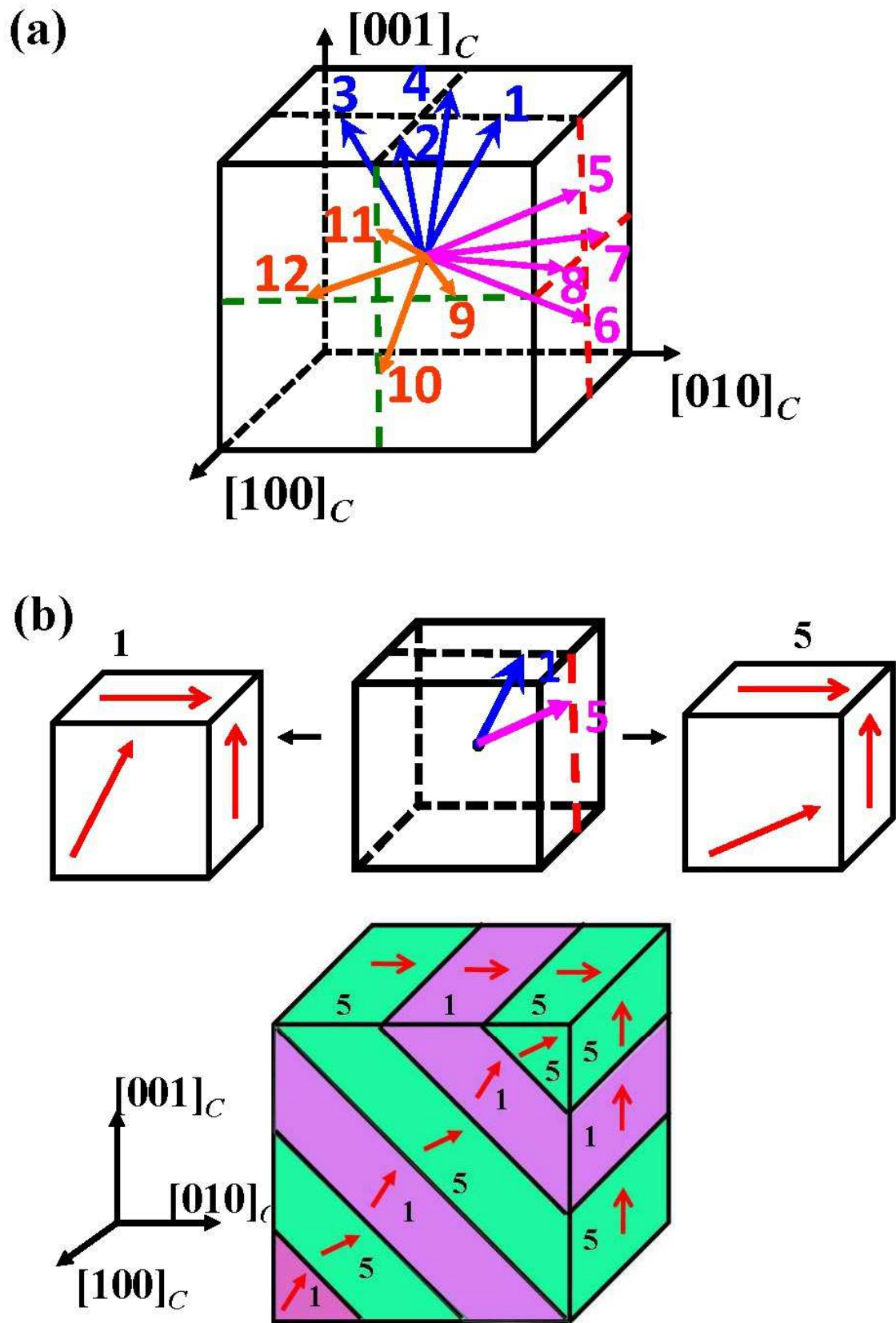
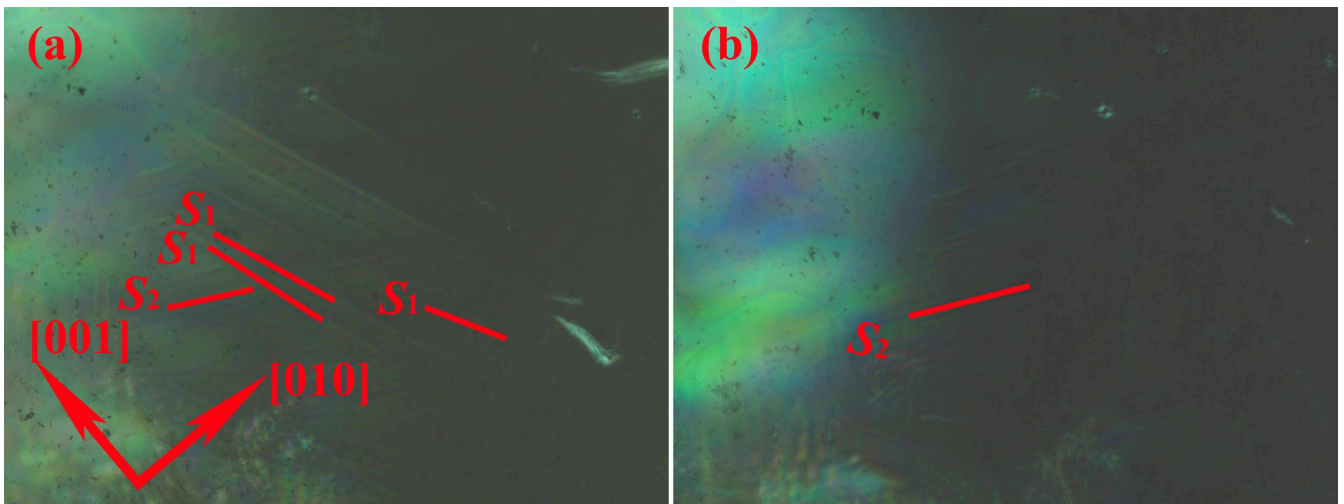


Figure 10 BB12509 12APR15



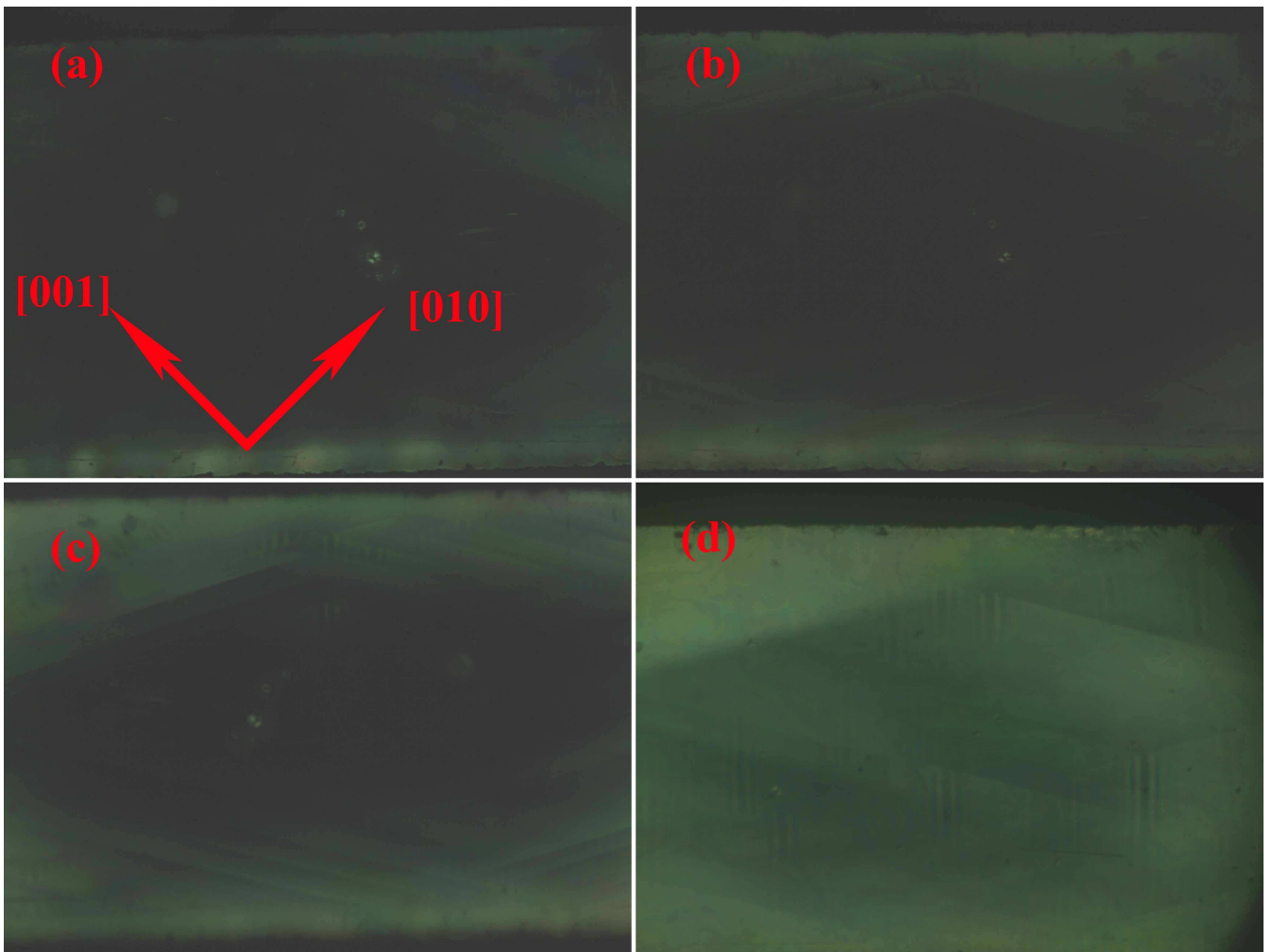


Figure 12

BB12509

12APR15

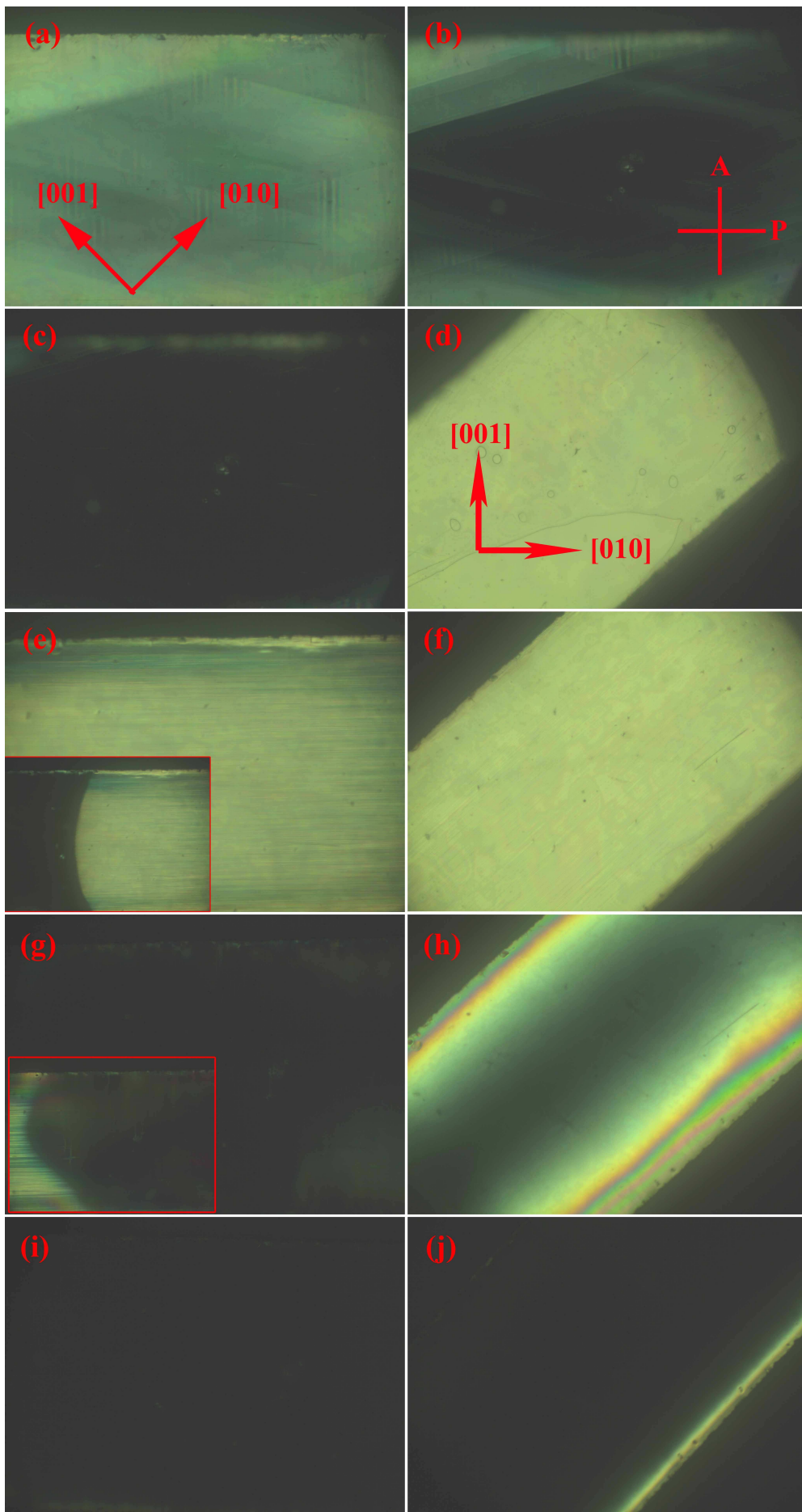


Figure 13 BB12509 12APR15

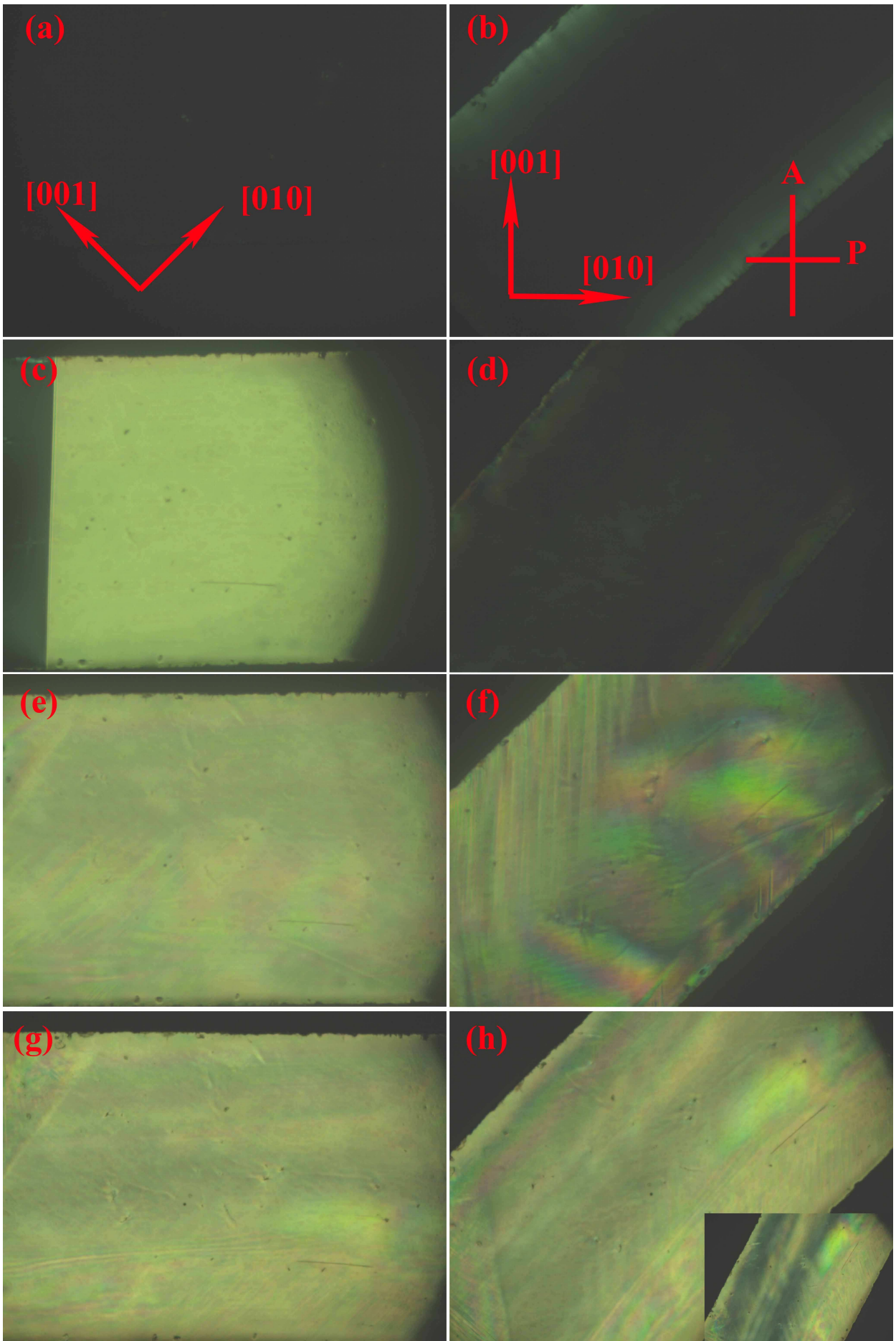


Figure 14 BB12509 12APR15

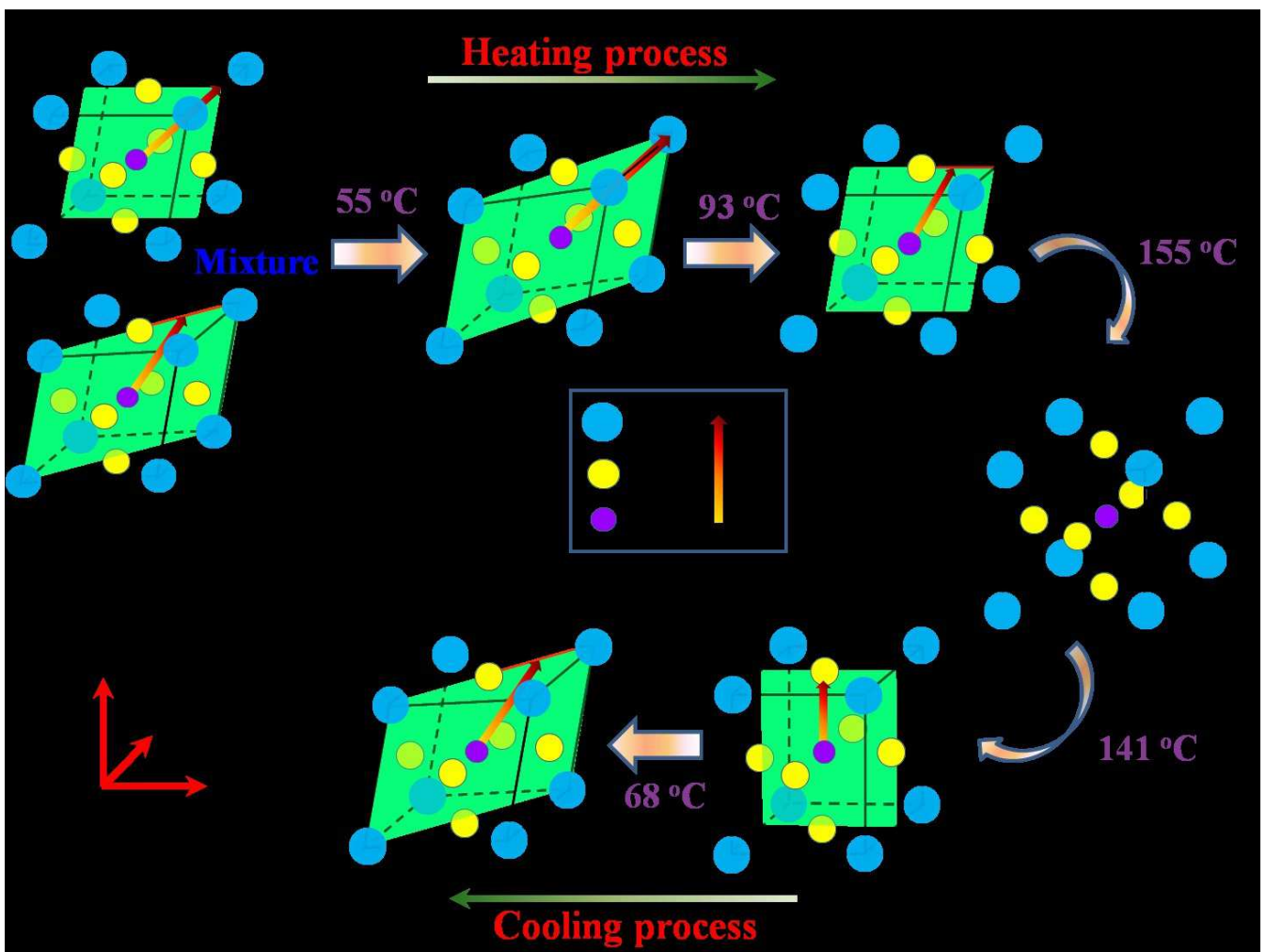


Figure 15

BB12509

12APR15